2023 EAGE ANNUAL 84TH CONFERENCE & EXHIBITION VIENNA | AUSTRIA

Receiver extension strategy using a time-dependent relocalization approach for time-domain FWI

M. Benziane[1], R. Brossier[1], L. Métivier[1,2]

[1] Univ. Grenoble Alpes, ISTerre; [2] Univ. Grenoble Alpes, CNRS, LJK

Summary

Full waveform inversion suffers from the cycle-skipping issue due to the non-linearity of the problem. In this work, we devise a new extension strategy of the FWI misfit function, in which we introduce additional degrees of freedom to the receiver position, generating receivers positions corrections which are time-dependent. This allows the fit multiple arrivals in the observed and calculated data. Our extension strategy aims at eliminating the kinematic mismatch at earlier FWI iterations, when the model estimate is poor, and conventional FWI is prone to cycle-skipping. The FWI gradient is computed using the corrected receiver position, giving a correct model update. This is implemented using nested loops optimization strategy, the outer loop solves for the model parameters using a quasi-Newton strategy, while the inner loop solves for the optimal receiver position correction time profiles, using a simulated annealing method. We constrain the receiver position, and the receiver speed by introducing penalty terms to the FWI problem.

A simple numerical experiment shows that a fit for two arrivals can be obtained, showing an improvement on the FWI gradient compared to conventional FWI and time-independent receiver extension. Lastly, we show the effect our strategy has on the convexity of the misfit function.

Receiver extension strategy using a time-dependent relocalization approach for time-domain FWI

Introduction

Full waveform inversion (FWI) aims at reconstructing the subsurface parameters in order to explain the entirety of the seismic waveforms. It is solved by iteratively improving the fit between the calculated and the observed data, using a local optimization scheme. The non-linearity of the forward modeling operator with respect to the model parameters causes the least-squares misfit function to be non-convex. Therefore, the convergence to a meaningful solution strongly depends on the starting model. This is the well known problem of cycle skipping (Virieux and Operto, 2009), which occurs when the time shift between the observed and calculated data is larger than half the dominant wavelength. Strategies to circumvent this issue have been investigated for a long time with various approaches (Bunks et al., 1995; van Leeuwen and Mulder, 2010; Métivier et al., 2016; Luo and Sava, 2011; Symes, 2008; van Leeuwen and Herrmann, 2013)). In this study we are interested in extension strategies, where additional degrees of freedom are introduced to help fit the data at earlier iterations of FWI, which are reduced gradually along the convergence path. Métivier and Brossier (2022) have proposed a receiver extension strategy, where one additional degree of freedom is introduced at each receiver position (for each source). This approach estimates the best horizontal spatial shift for each receiver (fixed in time), in order to compensate for the kinematic mismatch of the velocity model and fit the data when the model estimate is poor. This approach has showed promising results in several two-dimensional tests. However, it is noted that a fit for multiple arrivals may not be obtained with a constant spatial receiver shift: this is due to the time-independent receiver position correction that is driven by the arrival with the largest amplitude, while other weaker arrivals may require different position correction values. The purpose of the present study is to introduce a time-dependency to the receiver position correction, facilitating the fit of multiple arrivals at the earlier stages of FWI iterations.

Formalism

We write the receiver-extension problem

$$\min_{m,\Delta r_s} f(m,\Delta r_s) = \frac{1}{2}\sum_{s=1}^{N_s} ||R(x_r+\Delta r_s)u_s[m] - d_{obs,s}||_{\mathcal{D}}^2 + \frac{\alpha}{2}\sum_{s=1}^{N_s}\frac{||d_{obs,s}||_\infty^2}{L^2}\Delta r_s^2, \tag{1}$$

where

$$A(m)u_s = b_s, \tag{2}$$

and

$$R(x_r+\Delta r_s)u_s = \int_\Omega \delta(x-(x_r+\Delta r_s))u_s[m](x,t)dx. \tag{3}$$

The first term on the right hand side in equation (1) is the conventional least-squares misfit function. The wavefield $u_s[m]$ is the solution to the wave equation (equation 2), where $A(m)$ is the forward modeling operator and b_s is the source term. $R(x_r+\Delta r_s)$ is the restriction operator, which is a linear operator that extracts the calculated data from the wavefield at the receiver position $(x_r+\Delta r_s)$ as shown in equation (3). x_r is the true receiver position, while Δr_s is the receiver position correction. The term $R(x_r+\Delta r_s)u_s[m]$ is therefore the corrected calculated data. The second term in equation (1) is the least squares annihilator, it penalizes large values of receiver position correction. L is the maximum allowed receiver position correction and α is a tuning parameter. The larger the α value is, the closer is the solution to the original receiver position. If α tends to ∞ the misfit function shown in equation (1) becomes the conventional L_2 misfit function.

The receiver extension FWI is solved by using nested loops optimization approach. The outer loop solves for the model parameters using a quasi-Newton strategy (Nocedal and Wright, 2006), while the inner loop solves for the optimal receiver position to correct the kinematic mismatch of the velocity model, using a global optimization strategy. Métivier and Brossier (2022) use grid-search for this purpose.

For the outer loop, the gradient of the misfit function with respect to the model parameters is computed thanks to the ajdoint-state strategy (Plessix, 2006). An adjoint field (λ in equation 4) is computed backward in time using the forward modeling operator, and taking the residuals (μ_s in equation 4) as the source term, which are injected at the corrected receiver position as follows

$$\begin{cases} A(m)^T\lambda = R^T(x_r+\Delta r_s)\mu_s \\ \mu_s = d_{obs,s} - R(x_r+\Delta r_s)u_s \end{cases}. \tag{4}$$

The gradient is obtained by computing the inner-product of the scaled incident and adjoint wavefields:

$$\frac{\partial f}{\partial m} = \left\langle \frac{\partial A}{\partial m}u_s, \lambda_s \right\rangle. \tag{5}$$

In order to account for multiple arrivals, we introduce in this work a time-dependency to the receiver position. The receiver moves as a function of the simulation time in order to fit the multiple arrivals. We generate receiver position correction time profiles by decomposing the time vector into segments, each of which is represented by a polynomial (we use Lagrange polynomials). We write the receiver position correction time profile for a segment k

$$\Delta r_k(t) = \sum_{i=1}^{N+1} a_i \ell_i^N(t), \quad where \;\; \ell^N(t) \; are \; Lagrange \; basis \; functions \; of \; order \; N. \tag{6}$$

The inner loop is solved as determining the values at the control points (a_i in equation 6). To this purpose, we use Very Fast Simulating Annealing –VFSA– (Ingber, 1993). The new extended problem writes

$$\begin{aligned} \min_{m,\Delta r_s} f(m,\Delta r_s) = \frac{1}{2}\sum_{s=1}^{N_s} ||R(x_r+\Delta r_s(t))A(m)^{-1}b_s - d_{obs,s}||_{\mathcal{D}}^2 + \frac{\alpha}{2}\sum_{s=1}^{N_s}\frac{||d_{obs,s}||_\infty^2}{L^2}||\Delta r_s(t)||^2 + \\ \frac{\beta}{2}\sum_{s=1}^{N_s}\frac{||d_{obs,s}||_\infty^2}{V_{max}^2}||\frac{d\Delta r_s(t)}{dt}||^2. \end{aligned} \tag{7}$$

The receiver position correction is now time-dependent (equation 7). The adjoint source for the gradient computation in the outer loop is moving as a function of time. If the receiver moves too fast, Doppler effects can be observed. Therefore, we add in equation (7) a second penalization term to mitigate the velocity of receiver shift (first time derivative of the receiver position correction). V_{max} and β in equation (7) are the maximum allowed receiver speed and an other tuning parameter, respectively. The norms $||\Delta r_s(t)||$ and $|||\frac{d\Delta r_s(t)}{dt}||$ in equation (7) are computed using Gauss-Legendre quadrature rule. We note that if β tends to ∞, the problem reduces to the time-independent receiver extension strategy introduced by Métivier and Brossier (2022).

Ray theory analysis of a simple example

We conduct a simple ray theory analysis using a half-space model with one layer (Fig. 1a). We consider two arrivals, transmitted and reflected. Writing the travel time expression of the reflected arrival for a wrong velocity model v_1, at the corrected receiver position, and equating it to the travel time obtained at the true velocity v_0 using the original receiver position, gives a second order algebraic equation:

$$(\Delta r_x + x)^2 + (\Delta r_z + 2h)^2 = (4h^2 + x^2)\frac{v_1^2}{v_0^2}. \tag{8}$$

Similarly for the transmitted arrival:

$$(\Delta r_x + x)^2 + \Delta r_z^2 = x^2\frac{v_1^2}{v_0^2}. \tag{9}$$

In equations (8) and (9), h is the depth to the reflector and x is the offset. Equation (8) is a circle showing the possible receiver position corrections for which a fit for the reflected arrival can be obtained. It is centered at the image of the source with respect to the reflector, the radius of which is the square root of the right hand side of equation (8). Equation (9) is also a circle showing the possible receiver position corrections that give a fit for the transmitted arrival. It is centered at the source position, with a radius equal to the square root of the right hand side of equation (9). We plot the possible corrected receiver positions for the reflection and transmission cases (Figures 1b and 1c). In this example, the true velocity in the first layer is $v_0 = 2000$ m.s^{-1}, and we look at three different starting velocities (v_1 in Figures 1b and 1c). It is clear that a solution for the inner loop problem exists for this simple case. Two different receiver position corrections are necessary in order to obtain a fit for both arrivals. In the present study, we do not use horizontal receiver position correction only, even though it is sufficient to obtain a fit for the transmitted arrival (Fig. 1c), it is not the case for the reflected arrival when the velocity is lower than the true value (Fig. 1b). Therefore, we add a vertical component to the receiver position correction, in a manner that if the receiver moves toward the source, we have $\Delta r_z(t) = |\Delta r_x(t)|$, otherwise it moves horizontally. Imposing this relationship between vertical and horizontal corrections reduces the number of degrees of freedom of the inner loop significantly.

Numerical experiment

To illustrate our strategy, we consider a surface acquisition set-up, with a homogeneous first layer and a higher velocity half-space. The true velocity in the background is set to 2000 m.s^{-1}, while in the half-space it is set to 3500 m.s^{-1}. We keep the half-space at the correct velocity for the starting model, while the velocity in the first layer is set to 2200 m.s^{-1}. In Figure 2c the source and receiver used for this example are shown as a star and a triangle, respectively. The time shift between the observed and

the calculated data obtained at the original receiver position (d_{cal} is shown in a dashed line in Figure 2a) causes cycle-skipping.We show that the kernel for the conventional FWI is negative in the first Fresnel zone (black arrow in Figure 3a) suggesting a positive velocity perturbation to an already higher velocity. Using a time-independent receiver-extension mitigates this issue, the fit of the first arrival is obtained (d_{cal} is shown in blue in Figure 2a) yielding a kernel with the correct sign in the first Fresnel zone (black arrow in Figure 3b). However, the second arrival is not fitted, one can clearly see two migration isochrones (red arrow in Figure 3b), as well as the wrong velocity update in the rabbit-ears (blue arrow in Figure 3b). Using the time-dependent relocalization gives a fit for both arrivals (Fig. 2a), only one migration isochrone can be seen (red arrow in Figure 3c), and the rabbit ears are clearly visible in the time-dependent case and with the correct sign (blue arrow in Figure 3c) thanks to the fit of the reflected arrival.

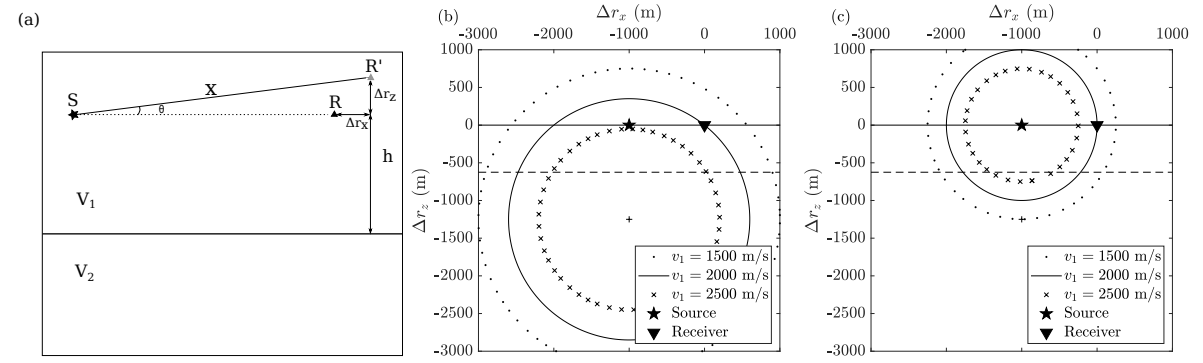

Figure 1 *Simple reflection case analysis with receiver extension. The geometry is shown in (a), R and R' are the original and extended receiver positions, respectively. Δr_x and Δr_z are the horizontal and vertical receiver position corrections. The possible receiver corrections at different velocities for the reflection and transmission cases are shown in (b) and (c), respectively.*

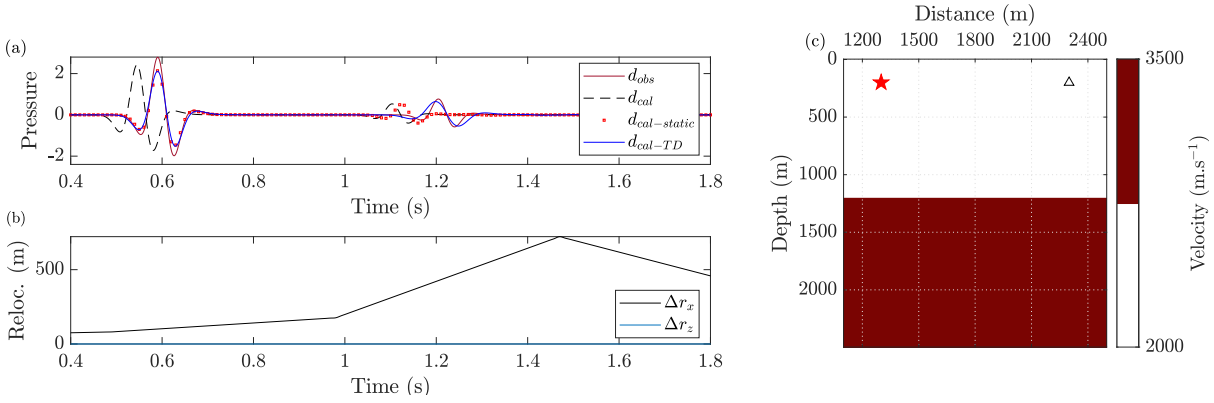

Figure 2 *Receiver extension for one source/receiver couple. (a) shows the observed data in brown, the calculated data at the original receiver position in a dashed line, and at the extended receiver, the time-independent and time-dependent cases are shown in red squares and in blue line, respectively. (b) Shows the time dependent relocalization profiles. (c) Set-up for the numerical experiment.*

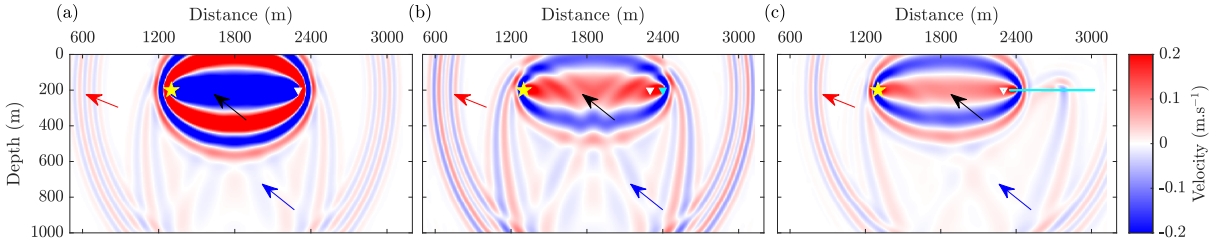

Figure 3 *FWI kernels, (a) at the original receiver position, (b) at the extended receiver using time-independent relocalization and (c) using time-dependent relocalization. The source is shown as a yellow star, the original and extended receivers are shown as a black and cyan triangles, respectively. The cyan line in (c) shows the range in which the receiver moves for the time-dependent case.*

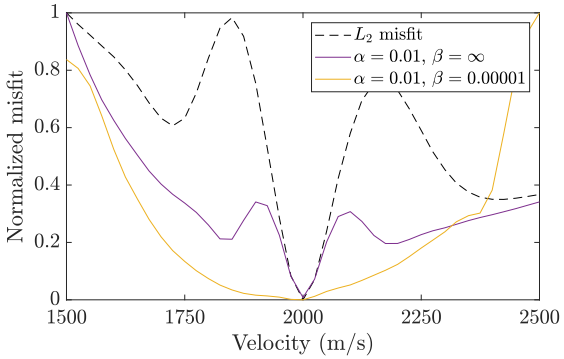

Figure 4 *Misfit function values computed at the different first layer velocities, the conventional least-squares misfit is shown in a dashed line. The misfit obtained using the time-independent and time dependent receiver extension strategies are shown in purple and yellow, respectively.*

It is interesting to look at the misfit function shape. For this example, we vary the velocity in the first layer (Fig. 2c) and compute the misfit for each velocity. The misfit function computed using the time-independent receiver extension is not convex in this two arrivals case (plotted in purple in Figure 4). Using the time-dependent receiver-extension strategy, described in this study, widens the valley of attraction and the misfit function shows improved convexity (shown in yellow in Figure 4). The effect of the second arrival fit is important.

Conclusion and perspectives

We devise a time-dependent receiver extension strategy for time-domain FWI, in order to account for multiple arrivals in the data. The first tests are promising and encourage further investigation and testing in realistic synthetic models. We consider currently extending our formulation to 3D, as well application for joint diving and reflected waveform inversion. Trans-dimensional optimization would be of interest for a more flexible parametrization of the inner problem.

Acknowledgements

This study was partially funded by the SEISCOPE consortium (`http://seiscope2.osug.fr`), sponsored by AKERBP, CGG, EXXON-MOBIL, GEOLINKS, JGI, PETROBRAS, SHELL, SINOPEC and TOTALENERGIES. This study was granted access to the HPC resources provided by the GRICAD infrastructure (https://gricad.univ-grenoble-alpes.fr), Cray Marketing Partner Network (`https://partners.cray.com`) and IDRIS/TGCC under the allocation 046091 made by GENCI.

References

Bunks, C., Salek, F.M., Zaleski, S. and Chavent, G. [1995] Multiscale seismic waveform inversion. *Geophysics*, **60**(5), 1457–1473.

Ingber, L. [1993] Simulated annealing: Practice versus theory. *Mathematical and Computer Modelling*, **18**(11), 29–57.

Luo, S. and Sava, P. [2011] A deconvolution-based objective function for wave-equation inversion. *SEG Technical Program Expanded Abstracts*, **30**(1), 2788–2792.

Métivier, L. and Brossier, R. [2022] Receiver-extension strategy for time-domain full-waveform inversion using a relocalization approach. *Geophysics*, **87**(1), R13–R33.

Métivier, L., Brossier, R., Mérigot, Q., Oudet, E. and Virieux, J. [2016] Measuring the misfit between seismograms using an optimal transport distance: Application to full waveform inversion. *Geophysical Journal International*, **205**, 345–377.

Nocedal, J. and Wright, S.J. [2006] *Numerical Optimization*. Springer, 2nd edn.

Plessix, R.E. [2006] A review of the adjoint-state method for computing the gradient of a functional with geophysical applications. *Geophysical Journal International*, **167**(2), 495–503.

Symes, W.W. [2008] Migration velocity analysis and waveform inversion. *Geophysical Prospecting*, **56**, 765–790.

van Leeuwen, T. and Herrmann, F.J. [2013] Mitigating local minima in full-waveform inversion by expanding the search space. *Geophysical Journal International*, **195(1)**, 661–667.

van Leeuwen, T. and Mulder, W.A. [2010] A correlation-based misfit criterion for wave-equation traveltime tomography. *Geophysical Journal International*, **182**(3), 1383–1394.

Virieux, J. and Operto, S. [2009] An overview of full waveform inversion in exploration geophysics. *Geophysics*, **74**(6), WCC1–WCC26.